Published January 30, 2017

Cardiolipin promotes electron transport between ubiquinone and complex I to rescue *PINK1* deficiency

Melissa Vos,[1,3,5] Ann Geens,[1,3] Claudia Böhm,[5] Liesbeth Deaulmerie,[1,3] Jef Swerts,[1,3] Matteo Rossi,[2,4] Katleen Craessaerts,[1,3] Elvira P. Leites,[6] Philip Seibler,[5] Aleksandar Rakovic,[5] Thora Lohnau,[5] Bart De Strooper,[1,3] Sarah-Maria Fendt,[2,4] Vanessa A. Morais,[1,3,6] Christine Klein,[5] and Patrik Verstreken[1,3]

[1]VIB Center for Brain and Disease Research, 3000 Leuven, Belgium
[2]VIB Center for Cancer Biology, 3000 Leuven, Belgium
[3]Department of Neurosciences and Leuven Research Institute for Neurodegenerative Disease and [4]Department of Oncology and Leuven Cancer Institute, KU Leuven, 3000 Leuven, Belgium
[5]Institute of Neurogenetics, University of Luebeck, 23562 Luebeck, Germany
[6]Instituto de Medicina Molecular, Faculdade de Medicina, Universidade de Lisboa, 1649 Lisboa, Portugal

PINK1 is mutated in Parkinson's disease (PD), and mutations cause mitochondrial defects that include inefficient electron transport between complex I and ubiquinone. Neurodegeneration is also connected to changes in lipid homeostasis, but how these are related to PINK1-induced mitochondrial dysfunction is unknown. Based on an unbiased genetic screen, we found that partial genetic and pharmacological inhibition of fatty acid synthase (FASN) suppresses toxicity induced by PINK1 deficiency in flies, mouse cells, patient-derived fibroblasts, and induced pluripotent stem cell–derived dopaminergic neurons. Lower FASN activity in *PINK1* mutants decreases palmitate levels and increases the levels of cardiolipin (CL), a mitochondrial inner membrane–specific lipid. Direct supplementation of CL to isolated mitochondria not only rescues the *PINK1*-induced complex I defects but also rescues the inefficient electron transfer between complex I and ubiquinone in specific mutants. Our data indicate that genetic or pharmacologic inhibition of FASN to increase CL levels bypasses the enzymatic defects at complex I in a PD model.

Introduction

Recessive mutations in phosphatase and tensin homologue–induced kinase (*PINK1*) cause early-onset Parkinson's disease (PD), an incurable neurodegenerative movement disorder (Valente et al., 2004). When mitochondria are stressed, PINK1 recruits Parkin to promote the autophagic clearance of mitochondria, and genetically PINK1 operates in this context upstream of Parkin (Clark et al., 2006; Park et al., 2006; Narendra et al., 2010). Also under nonstressed, endogenous conditions, the loss of PINK1 results in mitochondrial defects. These defects include reduced ATP levels, cristae defects, and a less negative mitochondrial membrane potential. Important aspects of these phenotypes can be explained by the inability of *PINK1* mutants to maintain phosphorylation of serine 250 in subunit NdufA10 of complex I in the electron transport chain (ETC). This defect results in inefficient electron transfer between complex I and ubiquinone in *PINK1* mutant fruit fly–, mouse-, and patient-derived cells (Clark et al., 2006; Park et al., 2006; Yang et al., 2006; Gautier et al., 2008; Morais et al., 2009, 2014; Vos et al., 2012). Hence, activation of pathways that increase ETC activity may bypass this electron transfer defect in *PINK1* mutants (Vos et al., 2012, 2013) and may constitute a promising therapy for PD.

Changes in lipid content are associated with aging and with neurodegeneration, including Alzheimer's disease and neurodegeneration with brain iron accumulation (Filippov et al., 2012; Aoun and Tiranti, 2015; Jazvinšćak Jembrek et al., 2015). Likewise, alterations in lipid metabolism have been described in models of PD as well (Lim et al., 2012; Tyurina et al., 2015). However, whether the mitochondrial dysfunction in *PINK1* mutants is under the control of specific changes in lipid content has not been investigated, nor has it been thoroughly explored whether mitochondrial dysfunction can be modified by alterations in lipid content.

In this study, we present an unbiased genetic screen and identify fatty acid synthase (FASN) as a dominant suppressor of PINK1 deficiency. Given the strong interest in FASN inhibition in the field of oncology, pharmacological inhibitors exist, and we show that they can also rescue PINK1 deficiency in fly-, mouse-, and patient-derived neurons, connecting the function of

Correspondence to Patrik Verstreken: patrik.verstreken@kuleuven.vib.be

Abbreviations used: CL, cardiolipin; CLS, CL synthase; ETC, electron transport chain; FASN, fatty acid synthase; iPSC, induced pluripotent stem cell; MEF, mouse embryonic fibroblast; PC, phosphatidyl choline; PD, Parkinson's disease; PE, phosphatidyl ethanolamine; PG, phosphatidyl glycerol; ROS, reactive oxygen species.

© 2017 Vos et al. This article is distributed under the terms of an Attribution–Noncommercial–Share Alike–No Mirror Sites license for the first six months after the publication date (see http://www.rupress.org/terms/). After six months it is available under a Creative Commons License (Attribution–Noncommercial–Share Alike 4.0 International license, as described at https://creativecommons.org/licenses/by-nc-sa/4.0/).

The Rockefeller University Press $30.00
J. Cell Biol.
https://doi.org/10.1083/jcb.201511044

Check for updates

THE JOURNAL OF CELL BIOLOGY

Downloaded from on February 15, 2017

Published January 30, 2017

FASN to the mitochondrial defects in *PINK1* mutants. Interestingly, among several changes in phospholipid levels in *PINK1* mutants, we show that the production of the mitochondrial-specific lipid, cardiolipin (CL), is inhibited. Our data indicate that CL, but not other phospholipids, plays a role in the regulation of electron transfer between complex I and ubiquinone. Our work suggests that CL regulates electron transfer in complex I and also indicates that strategies to increase CL levels are protective against mitochondrial dysfunction in *PINK1* mutants.

Results

Identification of FASN as dominant suppressor of PINK1 deficiency

In a genetic screen in fruit flies (Vos et al., 2012), we identified 10 ethyl methanesulfonate–induced mutations that dominantly suppress *pink1* mutant phenotypes. When heterozygous, these suppressors rescue decreased ATP levels, mitochondrial morphological defects, and the flying deficit of the $pink1^{B9}$-null mutant flies (Fig. 1 A). We used classical deficiency mapping and whole genome sequencing and found a nonsynonymous lesion in 7 of the 10 suppressor mutants (Fig. S1, A and B). One of them, *opa1*, had been previously identified as a *pink1* suppressor (Poole et al., 2008). The strongest *pink1* suppressor is a loss-of-function lesion in FASN2 (*FASN2/CG3524/v(2)k05816*; Fig. 1 A) and is specific to *pink1* because heterozygous *FASN2* loss only weakly suppresses *parkin*-null mutant phenotypes (Fig. S1 C). In addition, all the other *FASN2* alleles that we obtained also suppress the flight defects and the mitochondrial morphological defects in $pink1^{B9}$ mutant flies (Fig. 1, B–F; and Fig. S1, E and F). Note that heterozygous *FASN2* animals in an otherwise wild-type background ($pink1^{RV}$) did not show defects (Fig. 1, B–F; and Fig. S1, E and F). In addition, expression of wild-type FASN2 rescued the lethality of the different homozygous *FASN2* alleles we isolated, further indicating they are loss-of-function mutations (Fig. S1 D). Hence, partial loss of FASN2 rescues *pink1* mutant defects.

Pharmacological inhibition of FASN rescues PINK1-deficient flight defects and ATP levels

FASN is an evolutionarily conserved enzyme that catalyzes the synthesis of the free fatty acid palmitate (Fig. 2 A; Chirala and Wakil, 2004). Given the immense interest to inhibit FASN in oncology and metabolic disease (Menendez and Lupu, 2007; Ogino et al., 2008; Nguyen et al., 2010; Park et al., 2015), several inhibitors of this enzyme have been developed (Menendez and Lupu, 2007). Because inhibitors often have several off-target effects, we have tested three independent drugs, Cerulenin, Irgasan, and Orlistat, that block the second, sixth, and seventh steps of the FASN reaction, respectively (Fig. 2 A; Omura, 1976; Kapoor et al., 2004). When 1-d-old adult *pink1* mutant *Drosophila melanogaster* that display flight and mitochondrial defects were placed on medium with one of these compounds, the flies showed a progressive and dose-dependent improvement in flying, and their decreased ATP levels were significantly restored. No significant effect was observed in wild-type control flies that were fed with Cerulenin, Irgasan, or Orlistat (Fig. 2, C, E, and G). Hence, pharmacological inhibition of FASN rescues phenotypes in *Pink1*-deficient flies, and, in the remainder of our study, we used genetics and Cerulenin.

In addition to a rescue in flight and ATP levels, the characteristic mitochondrial clustering and blebbing defects of *pink1* mutant mitochondria in muscles of larvae were rescued after Cerulenin incubation (Fig. 3, A and B). Furthermore, Cerulenin also acutely restores a normal dense mitochondrial cristae structure in *pink1* mutant thorax muscles. We placed 1-d-old adult *Pink1* mutant animals that show mitochondrial cristae morphology defects on Cerulenin for 3 d and observed that the muscle tissue and mitochondrial morphology and cristae structure of *Pink1* mutants that were fed Cerulenin appeared much more like those in control thoraces (with or without Cerulenin), and they show much fewer signs of degeneration (Figs. 3 C and S2, A–C). Interestingly, the rescue we observe is specific for *Pink1*-induced phenotypes and not for *Parkin* because 1-d-old *Parkin* mutant flies that are on Cerulenin for 3 d are not rescued (Fig. S2 D). Although Pink1 and Parkin act together for some aspects of their function (Clark et al., 2006; Park et al., 2006; Narendra et al., 2009; Haddad et al., 2013), the effects of FASN inhibition appear to be specific for pathways under the control of Pink1 (Vilain et al., 2012; Pogson et al., 2014).

PINK1 rescue by FASN inhibition is evolutionarily conserved

To assess whether the rescue of Pink1-associated phenotypes by inhibition of FASN is evolutionarily conserved, we turned to $Pink1^{-/-}$-deficient mouse- and patient-derived cells. Incubation of $Pink1^{-/-}$ mouse embryonic fibroblasts (MEFs) or patient-derived fibroblasts with Cerulenin rescues the decreased ATP levels (Fig. 3, D and E). Compared with age-matched controls, dopaminergic neurons derived from induced pluripotent stem cells (iPSCs) from different *PINK1* carriers also displayed significantly lower ATP levels, although this effect was less pronounced than in the fibroblasts. Nonetheless, these lower ATP levels in *PINK1* mutant human dopaminergic neurons were also rescued when incubated with Cerulenin (Fig. 3 F). Hence, inhibition of FASN rescues PINK1 deficiency in flies and in mouse- and patient-derived cells.

Loss of FASN decreases palmitate levels in Pink1 deficiency

We used an enzyme-linked assay and measurement of optical density to assess free fatty acid levels that also include free palmitate. Genetic or pharmacological inhibition of FASN in flies and in MEFs showed a trend toward lower free fatty acid levels compared with controls, but the differences were statistically not significant (Fig. 4, A–C, two left bars). We then resorted to gas chromatography–coupled mass spectrometry to directly assess free palmitate levels and found that these were significantly lower in animals treated with Cerulenin (Fig. 4 D, two left bars), in line with the expected result when inhibiting FASN. Surprisingly, *pink1* mutants in the absence of FASN inhibition (Fig. 4 D, third bar) also showed a significant reduction in free palmitate levels. These levels were further reduced when *Pink1* mutants were treated with Cerulenin (Fig. 4 D, last bar).

The lower levels of free palmitate (and the trend toward lower free fatty acids) in *Pink1* mutants may at least partially be explained by our observation that *Pink1* mutant cells from mice and patients harbor lower FASN protein levels, as revealed by Western blotting (Fig. 4, E–H). It is well known that *Pink1* mutant cells harbor increased reactive oxygen species (ROS; He et al., 2008; Esposito et al., 2013). We therefore tested whether lower cellular FASN levels can be caused by increased ROS,

Downloaded from on February 15, 2017

Published January 30, 2017

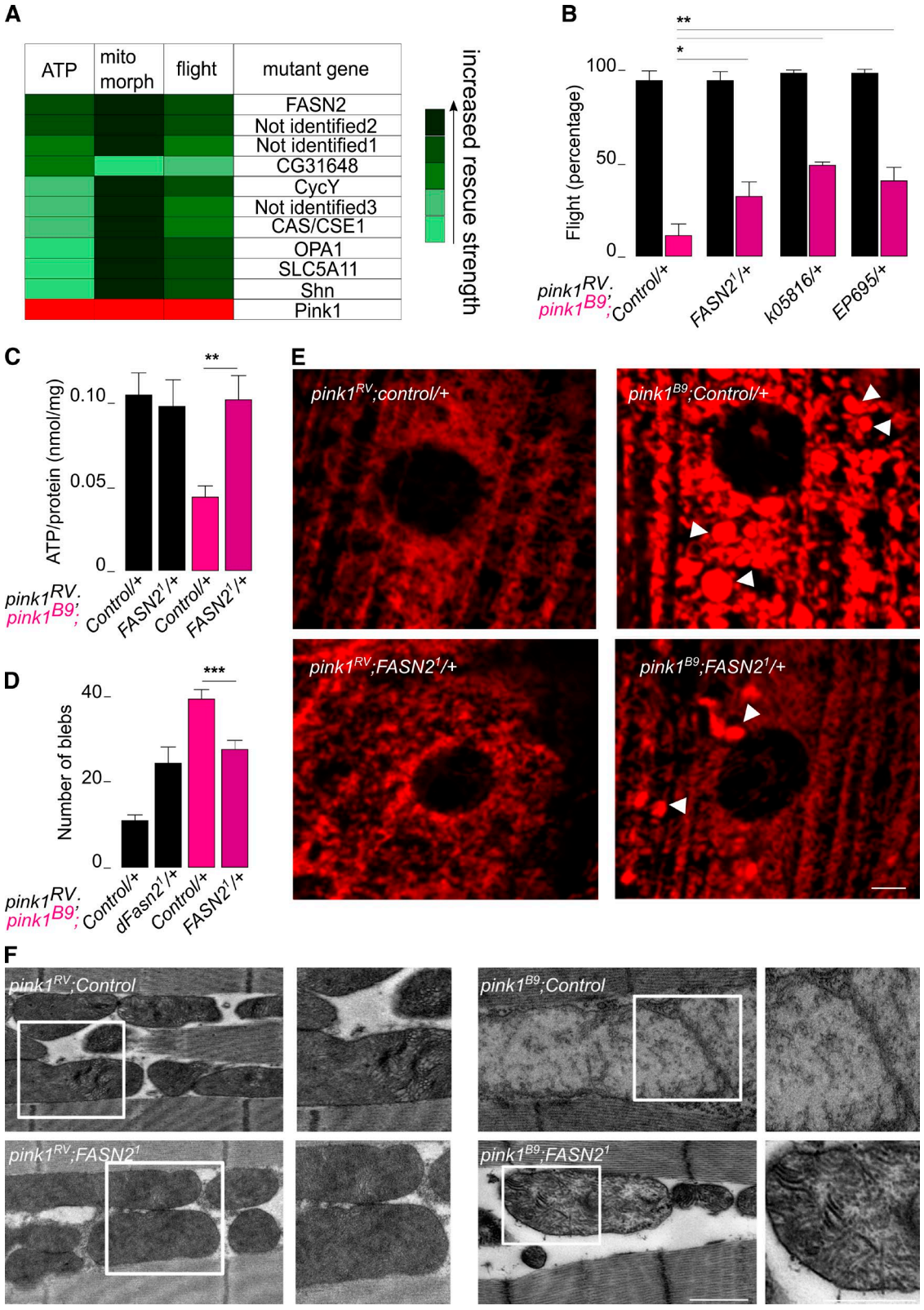

Figure 1. **Identification of *dFasn2* as a dominant suppressor of *pink1*^{B9}.** (A) Ranking of suppression levels of a phenotypic screen performed with 10 suppressors of *pink1*^{B9}, prioritizing rescue of ATP levels, then mitochondrial morphological defects, then flying ability. Green denotes significant rescue, whereas red denotes mutant phenotype (arbitrary scale). (B–F) Suppression of *pink1*^{B9} mutant phenotypes by *dFasn2/+* (pink bars) compared with *pink1*^{RV} controls heterozygous for *dFasn2* (black bars) using different *dFasn2* alleles for flight (n = 50 flies; B), ATP levels (n = 10 assays; C), mitochondrial morphology in muscles of third instar larvae (n = 20 muscle sections; D and E), and electron micrographs of adult thorax muscle mitochondria (n = 5 flies; F). Arrowheads in E denote mitochondrial aggregation (blebs). (B–D) Student's t test: *, $P < 0.05$; **, $P < 0.01$; ***, $P < 0.001$. Data represent percentages (B) or means (C and D) ± SEM. (E and F) Bars: (E) 5 µm; (F) 0.5 µm.

Downloaded from on February 15, 2017

Published January 30, 2017

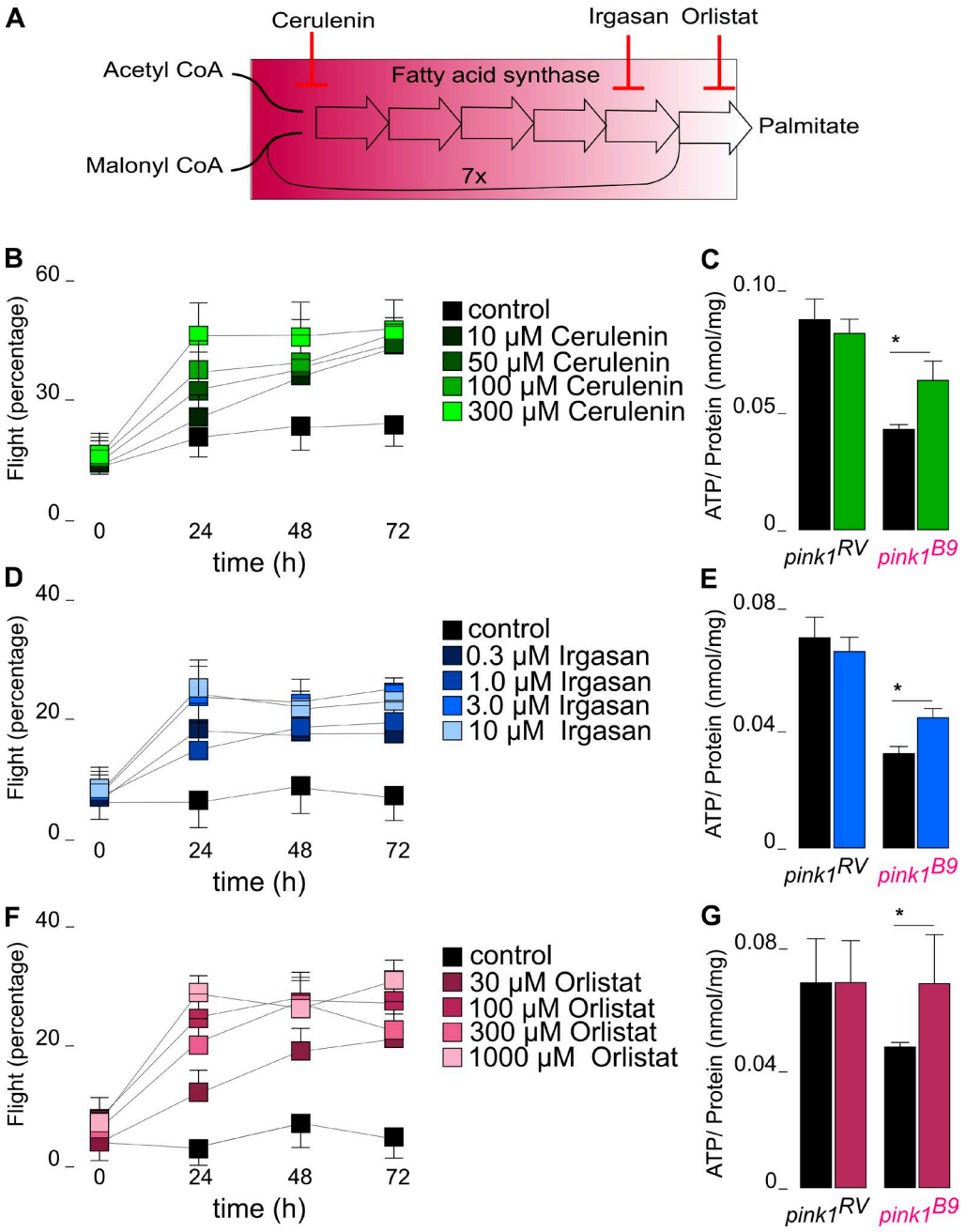

Figure 2. **Pharmacological inhibition of FASN rescues PINK1-deficient flight defects and ATP levels.** (A) Simplified schematic representation of the enzymatic reaction catalyzed by FASN requiring one Acetyl-CoA and seven Malonyl-CoAs to produce one palmitate in a seven-step enzymatic process. Compounds Cerulenin, Irgasan, and Orlistat block FASN at the second, sixth, and seventh steps, respectively. (B–G) Suppression of *pink1*^{B9} phenotypes by supplementing the fly medium with Cerulenin (green bars; B and C), Irgasan (blue bars; D and E), or Orlistat (pink bars; F and G) compared with control fly medium (black bars) for flying ability (n = 50 flies; B, D, and F) and ATP levels (n = 10 assays; 100 µM for Cerulenin, 3 µM for Irgasan, and 100 µM for Orlistat; C, E, and G). 1-d-old flies were selected and placed on the medium for 3 d before measuring ATP levels on 4-d-old flies. Student's t test: *, $P < 0.05$. Data represent percentages (B, D, and F) or means (C, E, G, and H) ± SEM.

and we treated MEF cells with H_2O_2. This manipulation indeed resulted in lower FASN protein levels (Fig. 4, I and J), indicating that increased ROS correlate with lower FASN protein levels (and thus with lower levels of free palmitate). Although *Pink1* mutants already show lower FASN levels and lower free palmitate levels than controls, this reduction is clearly insufficient to rescue the *Pink1*-associated defects. Yet, as we show here, further lowering FASN (either genetically or pharmacologically, resulting in both cases in lower free palmitate) does yield rescue of the phenotypes.

Inhibition of FASN increases CL levels in PINK1 mutants

Palmitate is involved in several downstream pathways, but this lipid also connects to mitochondrial function. Increasing the palmitate levels was shown to inhibit the production of CL, a lipid that is exclusive to the inner mitochondrial membrane and to the membranes of bacteria (Ostrander et al., 2001; Buratta et al., 2008). Unsaturated phosphatidyl glycerol (PG; not saturated PG) is a good substrate for CL synthase (CLS; Hoch, 1992; Rytömaa and Kinnunen, 1994; Bobyleva et al., 1997), and high

Downloaded from on February 15, 2017

Published January 30, 2017

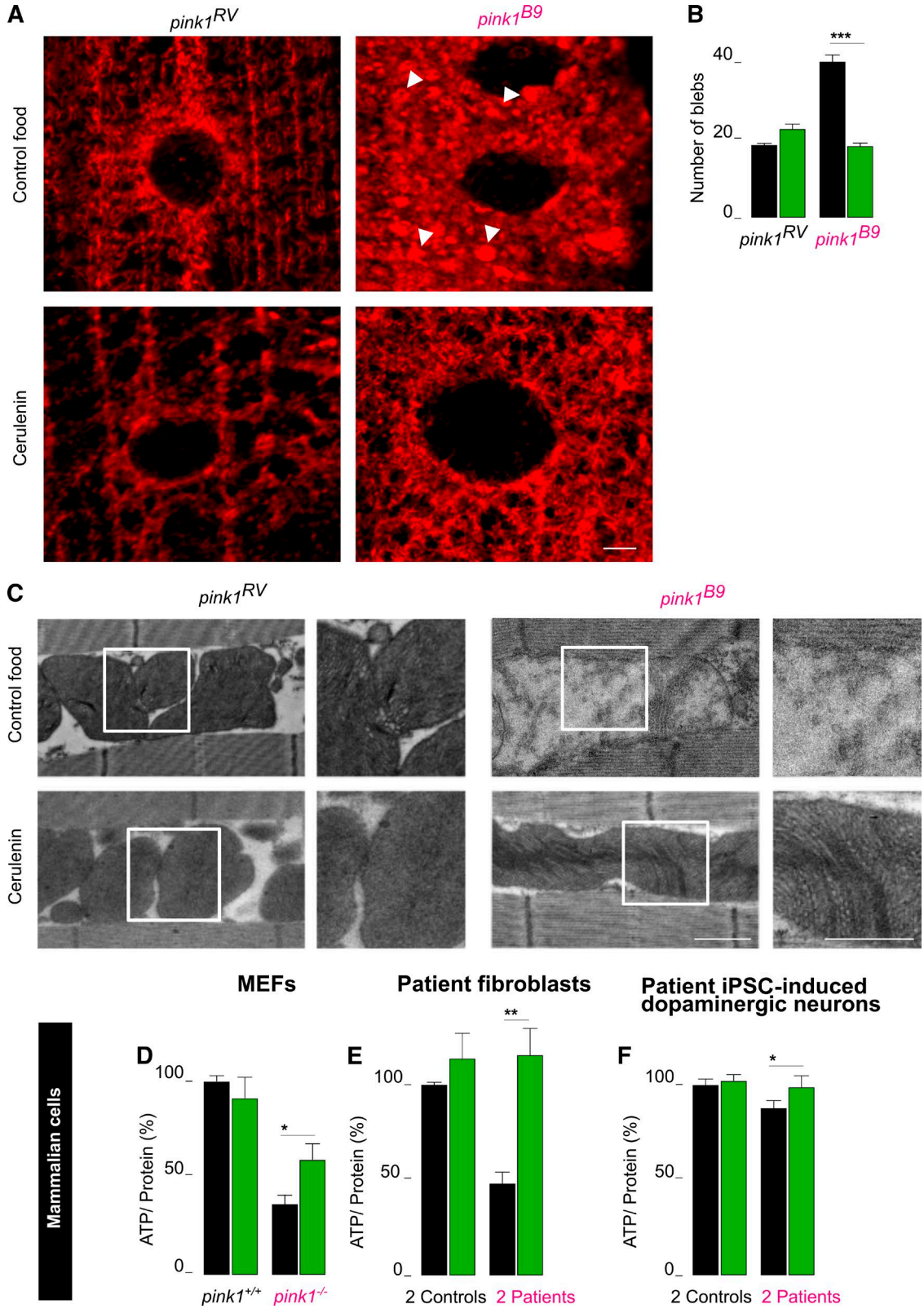

Figure 3. **The effect of FASN inhibition is evolutionarily conserved.** (A–C) Images (A) and quantification (B) of mitochondrial morphology (n = 20 muscle sections) in muscles of third instar larvae and electron micrographs of adult thorax muscle mitochondria (C; n = 5 flies) after Cerulenin incubation. Arrowheads in A denote mitochondrial aggregation (blebs). Boxes in C denote magnified areas. Bars: (A) 5 µm; (C) 0.5 µm. (D–F) ATP levels of *Pink1*$^{-/-}$ MEFs (n = 5 assays; D), patient fibroblasts (n = 5 assays of two independent control or patient lines; E), and dopaminergic neurons derived from iPSCs from patients (n = 3 assays of two independent control or patient lines; F) incubated with 10 µM Cerulenin (green bars) or with control medium (black bars). Student's t test: *, $P < 0.05$; **, $P < 0.01$; ***, $P < 0.001$. Data represent percentages (D–F) or means (B) ± SEM.

Downloaded from on February 15, 2017

Published January 30, 2017

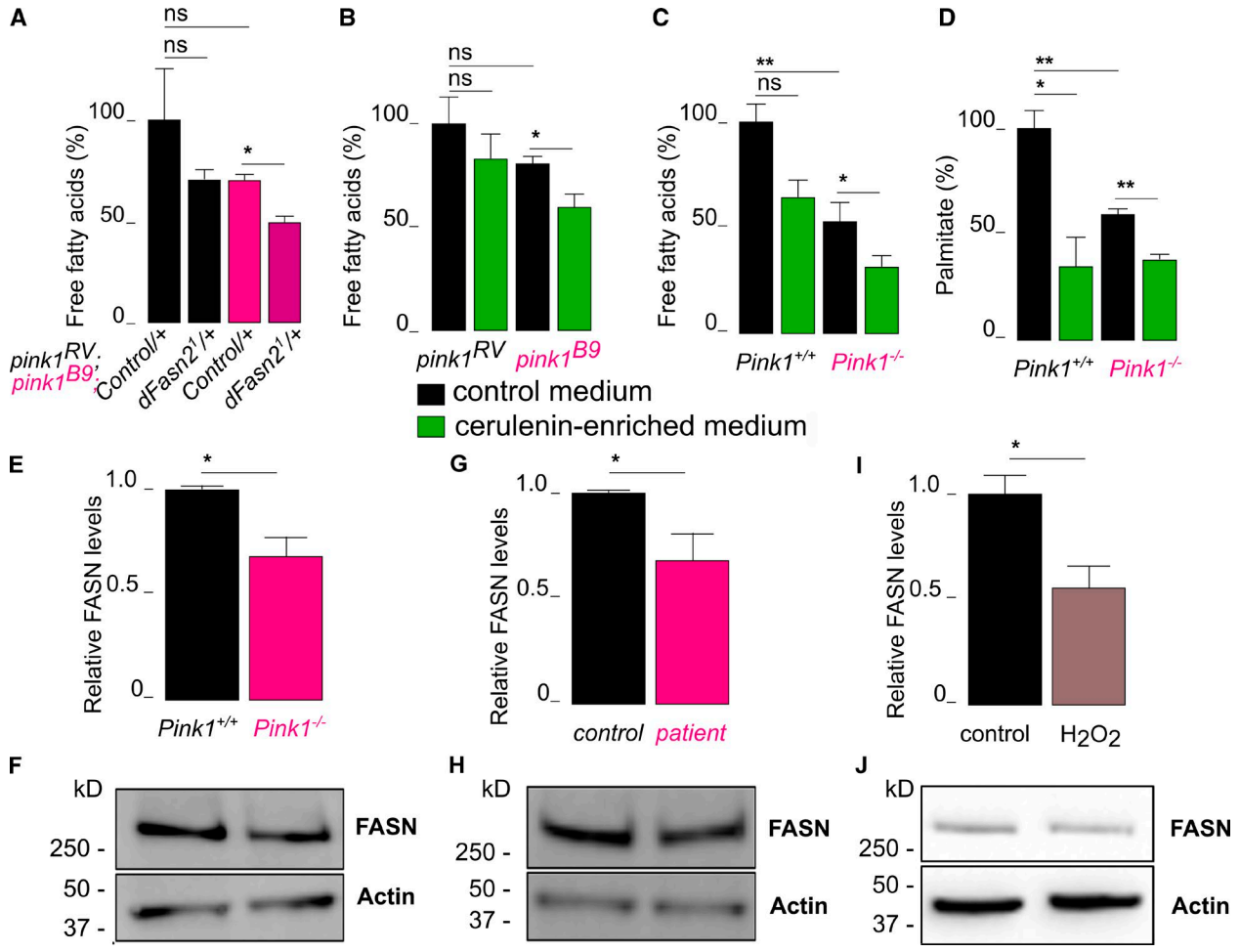

Figure 4. **Loss of FASN decreases palmitate levels in Pink1 deficiency.** (A and B) Free fatty acid levels are reduced in *pink1*^{B9} mutant flies and are further reduced by heterozygosity of *dFasn2* in *pink1*^{B9} mutant flies (pink; A) or by Cerulenin (green) in *pink1*^{B9} mutants (B) compared with *pink1*^{RV} control flies (black; $n = 5$ assays). (C and D) Free fatty acid levels (C) and palmitate levels (D) in *Pink1*$^{-/-}$ MEFs incubated with Cerulenin (green) are reduced compared with those not incubated with Cerulenin (black) and to *Pink1*$^{+/+}$ control MEFs. $n = 5$ assays. (E–J) Quantification (E, G, and I) and images (F, H, and J) of protein levels of FASN normalized to actin in *Pink1*$^{-/-}$ MEFs (E and F), patient-derived fibroblasts (G and H), and H_2O_2-treated wild-type MEFs (I and J). $n = 3$ assays. Bonferri's analysis of variance (A–D) and Student's *t* test (E, G, and I): *, $P < 0.05$; **, $P < 0.01$; ns, not significant. Data represent percentages (A–D) or normalized means (E, G, and I) ± SEM.

levels of palmitate shift the balance toward more saturated PG (Fig. 5 A; Ostrander et al., 2001). We used shotgun lipidomics and assessed PG levels in mitochondrial fractions of MEFs. Saturated PG levels were extremely low in controls and were below the detection limit in *Pink1* mutant samples. Assessing unsaturated PG levels, we found that inhibition of FASN resulted in a significant increase in most unsaturated PG species (Fig. 5 B). When inhibiting FASN, other lipid species were also expected to be affected. As indicated in Fig. S3, the differences we measured in isolated mitochondria from control cells with and without Cerulenin were not significantly different. Nonetheless, the lower palmitate levels and increased unsaturated PG that we detected upon inhibition of FASN are very robust and consistent with our model.

Pink1 mutants are known to harbor increased mitochondrial ROS (He et al., 2008; Esposito et al., 2013), and high ROS levels are known to result in decreased levels of CL (Ruggiero et al., 1992; Ellis et al., 2005). In line with this, CL levels in mitochondrial fractions of *Pink1*$^{-/-}$ MEFs were significantly decreased compared with control MEFs (Fig. 5, C and D). Next, we tested the effect of inhibiting FASN using Cerulenin that causes increased levels of unsaturated PG (see previous paragraph). We found that in *Pink1*$^{-/-}$ MEFs, the levels of all CL species measured were almost completely restored to control levels (Fig. 5, C and D). Hence, loss of FASN function results in more mitochondrial CL in *Pink1*$^{-/-}$ mutant MEFs.

Loss of FASN increases complex I function

PINK1$^{-/-}$ mutants show lower enzymatic activity of complex I (Gautier et al., 2008; Morais et al., 2009). We therefore wondered whether the rescue by inhibiting FASN acts through bypassing this complex I defect. We detected that partial inhibition of FASN using genetic or pharmacological tools restored the defective complex I enzymatic activity in *PINK1* mutant flies and in MEFs back to control levels (Fig. 6, A–C). The inefficient electron transport between complex I and ubiquinone in *PINK1* mutants was previously shown to be the result of an inability to maintain phosphorylation of Serine 250 in the complex I subunit NdufA10 (Morais et al., 2014). Indeed, mitochondria from engineered mammalian cells expressing only phosphorylation-deficient NdufA10^{S250A} transfer electrons less efficiently

Downloaded from on February 15, 2017

Published January 30, 2017

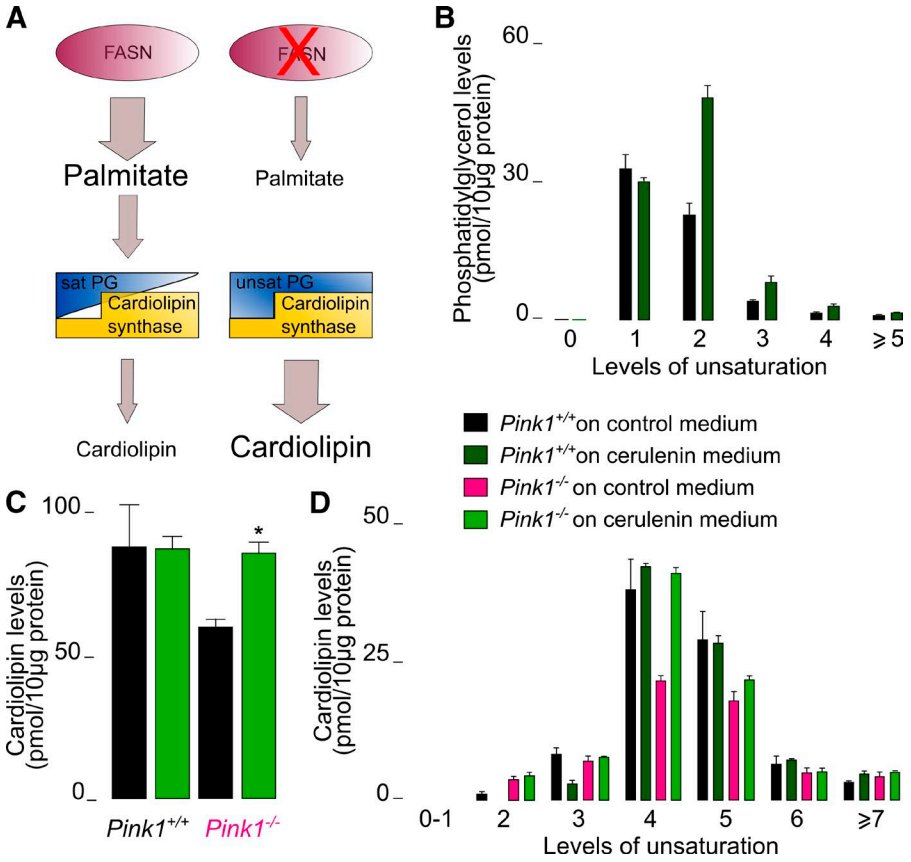

Figure 5. **Loss of Pink1 results in decreased CL levels.** (A) Palmitate produced by FASN promotes the formation of saturated PG that is a weak substrate for CLS, thus resulting in lower CL levels. Lower levels of palmitate upon inhibition of FASN shift the balance to increased levels of unsaturated PG, which serve as a strong substrate for CLS, thus producing more CL. (B–D) Shotgun lipid analysis of mitochondria isolated from *Pink1*$^{-/-}$ and *Pink1*$^{+/+}$ MEFs (n = 2 independent experiments) that were incubated with Cerulenin (green bars) compared with those incubated with control medium (black bars) for PG separated by side chain unsaturation levels (B), CL alone (C), and CL separated by side chain unsaturation level (D). Student's t test: *, $P < 0.05$. Data represent means ± SEM.

from complex I to ubiquinone, similar to *Pink1* mutant mitochondria (Fig. 6 D). Interestingly, we found that pharmacological inhibition of FASN resulted in a restoration of this activity (Fig. 6 D), indicating that the inhibition of FASN bypasses this ETC defect.

CL increases complex I function

Our data are consistent with a model wherein *Pink1* mutant mitochondrial dysfunction is rescued because the loss of FASN results in increased mitochondrial CL. We challenged this model by taking three independent approaches. In our first approach,

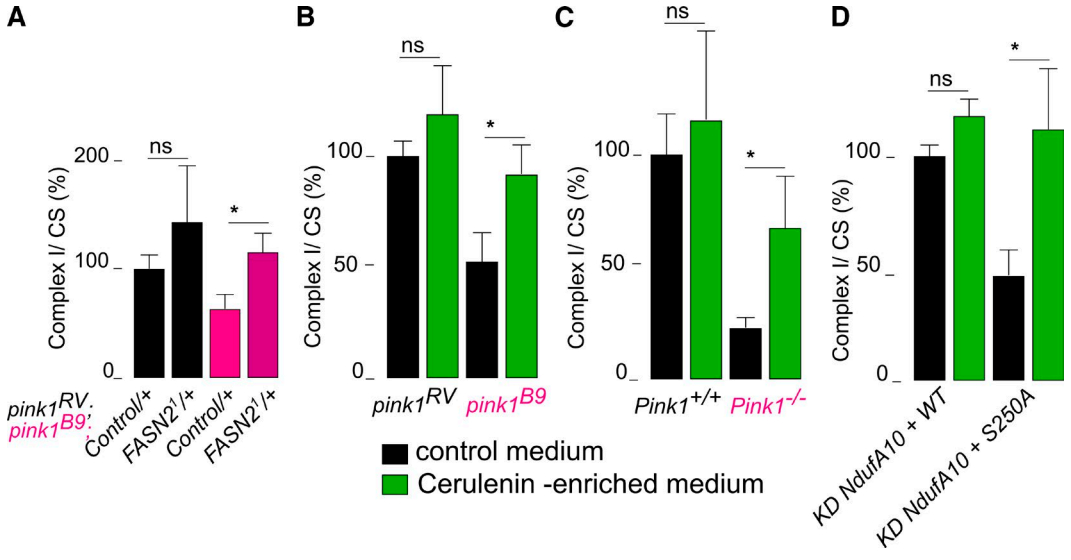

Figure 6. **Loss of FASN improves complex I activity upon Pink1 deficiency.** (A and B) Complex I activity normalized to citrate synthase (CS) in *pink1*^{B9} mutant flies that were rescued by heterozygous *dFasn2*^{1} in *pink1*^{B9} mutant flies (pink; A) or by inhibition of FASN by Cerulenin (green; B) in *pink1*^{B9} mutant flies compared with *pink1*^{RV} control flies (black). n = 8 assays. (C) Complex I activity normalized to citrate synthase in *Pink1*$^{-/-}$ MEFs incubated with Cerulenin (green) compared with those not incubated with Cerulenin (KD; black) and to *Pink1*$^{+/+}$ control MEFs. n = 5 assays. (D) Complex I activity normalized to citrate synthase in cells where NdufA10 was knocked down (Morais et al., 2014) and where wild-type NdufA10 (WT) or phosphorylation-deficient NdufA10 (S250A) are reexpressed and then incubated with Cerulenin (green) or control medium (black). n = 4 assays. Student's t test: *, $P < 0.05$; ns, not significant. Data represent percentages ± SEM.

Downloaded from on February 15, 2017

Published January 30, 2017

we fed flies an unrelated lipid, stearic acid, that was previously shown to rescue the climbing defect and lower ATP levels seen in *Pink1*-deficient flies (Senyilmaz et al., 2015). Unlike Cerulenin, stearic acid did not increase the activity of mitochondrial complex I in *Pink1* mutants (Fig. S4). These data indicate the specificity of our approach and suggest that stearic acid rescues aspects of the *Pink1* phenotype by acting through a different pathway than complex I (e.g., mitochondrial fission; Vilain et al., 2012; Senyilmaz et al., 2015).

In our second approach, we isolated mitochondria from *Pink1* mutant flies or *Pink1*$^{-/-}$ MEFs and incubated them with different amounts of various lipids, including PG, phosphatidyl ethanolamine (PE), phosphatidyl choline (PC), and CL, while sonicating, thus allowing the lipid to incorporate (Fig. 7, A–D). Only CL, and not PG, PE, or PC, showed a strong rescue of the electron transfer activity defects in complex I of *Pink1* mutants (Fig. 7, A–D). This effect was absent in control samples that underwent the same treatment and was also seen when using mitochondrial fractions from *Pink1*$^{-/-}$ MEFs (Fig. 7 E). Hence, directly supplementing *Pink1* mutant mitochondria with CL can bypass the complex I defect.

In a final approach, we scrutinized our model using genetics. CL is produced in mitochondria by CLS (Nowicki et al., 2005; Acehan et al., 2011), and we observed that partial loss of CLS (*CLS*^{e01021}/+) in fruit flies resulted in lower complex I activity compared with the complex I activity measured in control flies (Fig. 7 F). This defect in complex I activity in *CLS*/+ animals was not rescued by the inhibition of FASN with Cerulenin (Fig. 7 F, first green bar). In addition, the rescue of complex I defects in *Pink1* mutants by Cerulenin is lost in *Pink1* mutants that are also mutants for *CLS* (Fig. 7 F, right green bar). These data further support the model wherein the rescue of complex I defects in *Pink1* mutants by the inhibition of FASN follows a CL-dependent pathway.

CL stabilizes cristae and ETC supercomplexes (Pfeiffer et al., 2003; Friedman et al., 2015), but a role for this lipid in the direct regulation of electron transport between complex I and ubiquinone in animal mitochondria has not been assessed. As noted in the Loss of FASN increases complex I function section, electron transfer in *Pink1* mutant mitochondria is caused by defective NDUFA10 phosphorylation (Morais et al., 2014). We therefore tested the ability of CL to bypass the electron transfer defect in NdufA10^{S205A} phosphorylation-deficient cells. We incubated mitochondria from such cells with CL and found that this manipulation efficiently rescued the complex I defects (Fig. 7 G). Hence, CL facilitates electron transport between complex I and ubiquinone, and increasing CL levels are sufficient to bypass the defects in *Pink1* and *NdufA10*^{S205A} mutants.

Discussion

In this study, we present a previously uncharacterized function for the mitochondrial inner membrane lipid CL, and we show that increased CL rescues *Pink1*-induced mitochondrial dysfunction. CL has been coupled to the maintenance of mitochondrial cristae structure, and it is key to maintaining ETC supercomplexes (Pfeiffer et al., 2003). We now expand on this and provide evidence that CL also couples electron transfer between complex I and ubiquinone to increase the efficiency of the ETC. *Pink1* mutants and many sporadic PD patients suffer from such complex I defects. We find that *CLS* mutants show decreased electron transfer from complex I to ubiquinone; conversely, increasing CL levels by partial inhibition of FASN using genetics or pharmacology significantly rescues the mitochondrial defects in *Pink1* mutant cells (in both mice and patients) as well as in the degenerative phenotypes and flight defects in adult fruit flies. Loss of FASN also affects the levels of other lipids in isolated mitochondria. However, we did not observe an improvement in complex I activity after the incubation of isolated mitochondria with these lipids, suggesting that these changes in lipid level likely are not significantly contributing to the *PINK1* mutant phenotypes, as we report in this study.

Thus, our work also indicates specificity to CL, as the biochemical defect at complex I in *Pink1* mutants is not affected by other lipids, including PG, PE, PC, and stearic acid.

Our data are consistent with a significant contribution of ETC defects to *Pink1* pathology, but they also confirm that Pink1 acts in multiple parallel pathways. Stearic acid was recently shown to rescue *Pink1*-associated defects in fruit flies by activating pathways that induce mitochondrial fission (Senyilmaz et al., 2015). We and others previously showed that mitochondrial fission acts in parallel to a role of Pink1 in regulating complex I activity because increasing mitochondrial fission in *Pink1* mutants does not rescue their complex I defect (Vilain et al., 2012; Pogson et al., 2014). Similar to these findings, stearic acid treatment does not rescue the complex I defect of *Pink1* mutants. These observations are in contrast to those of increasing CL levels: CL does rescue the complex I dysfunction, but our EM study shows that mitochondria still appear somewhat enlarged, as was also seen previously when expressing a phosphomimetic NDUFA10^{S250D} in *Pink1* mutant animals (Morais et al., 2014). Although targeting either pathway significantly improves mitochondrial dysfunction such that the mutant flies can fly again, a strategy that targets both simultaneously may yield even stronger effects (Vilain et al., 2012).

Neurodegeneration and aging have been linked to changes in lipid composition. The lower CL levels may be the consequence of mitochondrial stress, including increased ROS that accumulate because of inefficient electron transport in complex I (He et al., 2008; Esposito et al., 2013). Although it is recognized that upon mitochondrial stress, CL is relocated to the outer mitochondrial membrane (Garcia Fernandez et al., 2002) to serve as a recognition signal for the degradation of mitochondria (Chu et al., 2013), the mitochondrial mass in *Pink1* mutant flies or cells is not particularly lower compared with wild-type controls (Rakovic et al., 2013). Rather, the defective mitochondria in *Pink1* mutants that are not degraded can be rescued by increasing CL levels, and this manipulation appears sufficient and specific to restore a dense cristae structure and to bypass the complex I dysfunction in *Pink1* mutants. Other phospholipids were not able to rescue the complex I defects like CL could, suggesting that these phospholipids do not significantly contribute to the rescue of complex I dysfunction in *PINK1* deficiency.

The loss of *Pink1* also correlates with lower palmitate levels. The production of palmitate by FASN requires a considerable amount of energy (Wakil et al., 1983), a feat particularly relevant in the context of *Pink1* mutants that harbor lower cellular ATP levels (Clark et al., 2006; Park et al., 2006). *Pink1*-defective cells may thus access other sources in an attempt to maintain free fatty acid levels. The lower FASN levels we observed in *Pink1* mutants and in H_2O_2-treated cells may be a protective mechanism under such conditions of low cellular energy, but further work is needed here. The palmitate mass that we measured in *Pink1* mutant samples may thus not be a simple reflection of direct cellular palmitate synthesis by FASN but a combination of

Downloaded from on February 15, 2017

Published January 30, 2017

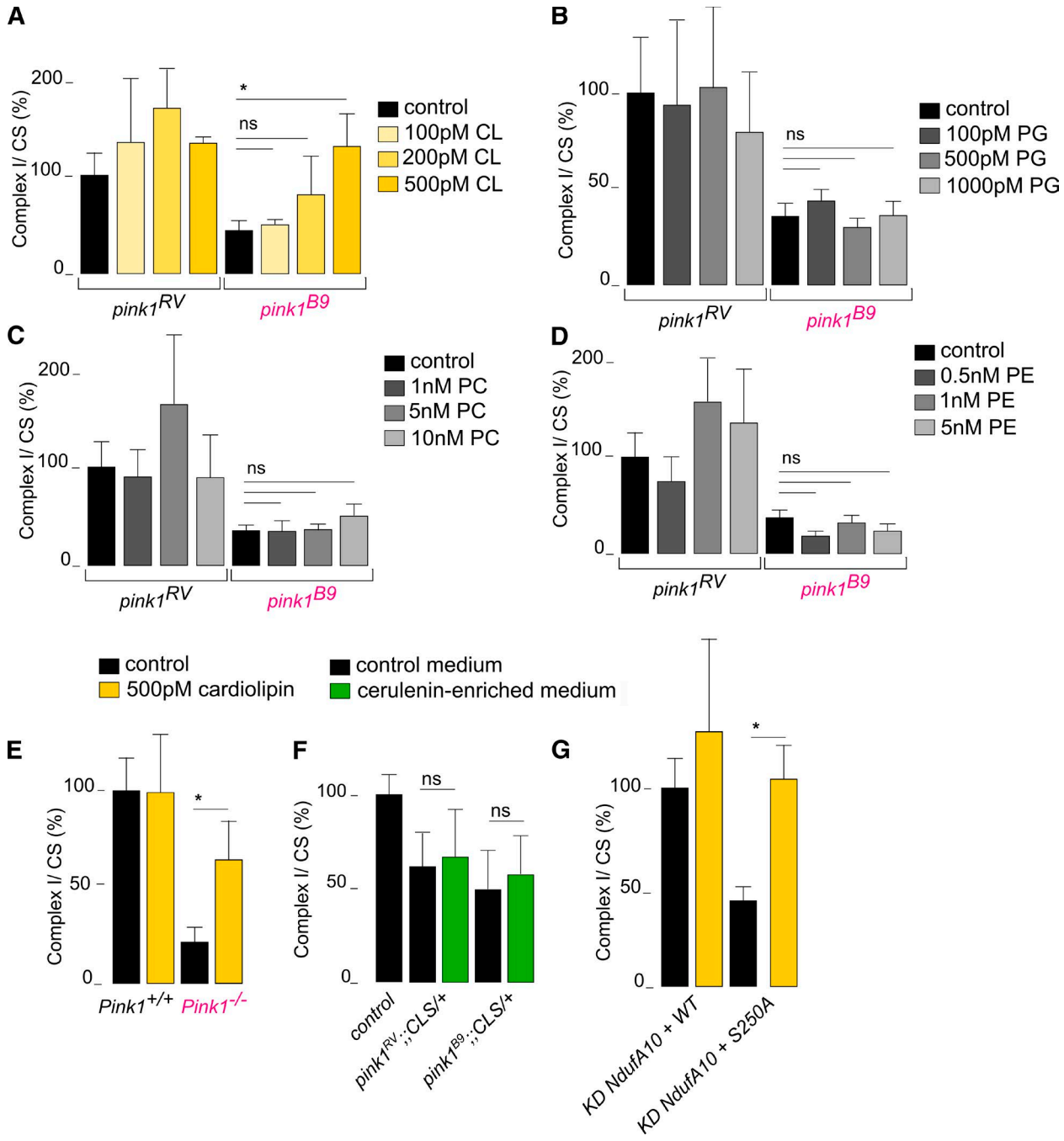

Figure 7. **CL couples electron transport between complex I and ubiquinone.** (A–D) Complex I activity normalized to citrate synthase (CS) in isolated mitochondria from *pink1* mutant flies and control flies after 60 min of sonication and incubation with different concentrations of CL (A), PG (B), PC (C), and PE (D). The phospholipids added include the fatty acyl chains that were observed in the lipidomics analysis for those specific lipids. (E) Complex I activity normalized to citrate synthase from isolated mitochondria from *Pink1*$^{-/-}$ and control *Pink1*$^{+/+}$ MEFs with 500 pM CL compared with control medium for 60 min. (F) Complex I activity normalized to citrate synthase of loss of CLS in control and Pink1-deficient flies. $n = 5$ assays. (G) Complex I activity normalized to citrate synthase after incubation and sonication of mitochondria isolated from cells where NdufA10 was knocked down and where wild-type NdufA10 (WT) or phosphorylation-deficient NdufA10 (S250A) were reexpressed. $n = 4$ assays. Student's *t* test: *, $P < 0.05$; ns, not significant. Data represent percentages ± SEM.

different contributing factors, such as lower uptake, less synthesis, and more consumption. These findings support the idea that inhibiting FASN in *Pink1* mutants not only restricts palmitate production, thus allowing more CL synthesis, but that this maneuver may, to some extent, also help to conserve cellular energy.

Thus, we propose that the lower FASN levels or activity may help to conserve energy and, more significantly, result in increased levels of CL to facilitate electron transfer between complex I and ubiquinone. FASN is a major target in oncology and metabolic disease, and phase I trials to inhibit the enzyme are ongoing. However, unlike the need to strongly inhibit the enzyme in oncology applications, our genetic work predicts that in PD, partial inhibition is sufficient, thereby reducing the risk of side effects.

Downloaded from on February 15, 2017

Published January 30, 2017

Materials and methods

Fly genetics

w pink1^{B9} (FBgn0029891) and *park^{1}* (FBgn0041100) mutant and *w pink1^{RV}* and *park^{RV}* control flies were provided by J. Park and J. Chung (Korea Advanced Institute of Science and Technology, Daejeon, South Korea; Cha et al., 2005; Park et al., 2006), *park$^{\Delta 21}$* mutants were provided by G. Mardon (Baylor College of Medicine, Houston, TX; Pesah et al., 2004), and UAS-Fasn2 was provided by J. Montagne (Université Paris-Sud, Orsay, France; Garrido et al., 2015). Deficiencies and P-element mutants were from the Bloomington Drosophila Stock Center (Bier et al., 1989; Ashburner et al., 1990; Spradling et al., 1999; Mason et al., 2004; Parks et al., 2004; Ryder et al., 2007). *dFasn2^{1}* is *y w eyFLP.GMR::LacZ; dFasn^{1} P[y^{+}] P[FRT40A neo^{+}]* and control is *y w eyFLP GMR::LacZ; P[y^{+}] P[FRT40A neo^{+}]* (Verstreken et al., 2005). *k05816* (FBgn0042627) is *y^{1} w^{67c23}; P{lacW}FASN2^{k05816}/CyO* and *EP695* is *w^{1118}; P{EP}FASN2^{EP695}/CyO*. The 10 ethyl methanesulfonate screen mutants are *y w eyFLP GMR::LacZ; P[y^{+}] P[FRT40A neo^{+}] *mutant* (Verstreken et al., 2005). *CLS* flies are *w^{1118}; PBac{RB}CLS^{e01021}/TM6B, Tb^{1}*.

Cells

Pink1$^{-/-}$ MEFs were previously described (Morais et al., 2009). In brief, heterozygous *Pink1* knockout mice (*Pink1$^{+/-}$*) were interbred to generate mutant mice and wild-type littermate controls. At embryonic day 13, embryos were dissected into cell culture dishes containing DMEM supplied with 50% FCS and 1% penicillin/streptomycin. Cultures were expanded and serum concentration was constantly decreased to 10% FCS after they reached consistent growth. Afterward, the cultures were immortalized by transfection with SV40 large T antigen.

The NdufA10 HeLa cells were described and characterized previously (Morais et al., 2014). In brief, the HeLa NdufA10 downregulated cell line was generated using shRNA against human NdufA10 (targeted sequence, 5′-CAGAAGAAAGGAGATCCACATGAAATG AA-3′) according to the supplier's protocol (OriGene) and were selected based on their acquired puromycin resistance.

We have studied fibroblast cultures from two *PINK1* mutation carriers harboring homozygous p.Q456X and p.V170G mutations (female, mean age 80 ± 0.7 yr; mean age at onset: 46 ± 21 yr). In addition, two cultures from healthy control individuals were included (female, mean age 51 ± 4.9 yr) that are family members from the patient carrying the p.Q456X mutation (Grünewald et al., 2009).

The iPSC lines were differentiated into dopaminergic neurons as described previously (Kriks et al., 2011; Munsie et al., 2015). In brief, iPSC colonies were dissociated into single cells using accutase (Thermo Fisher Scientific) and replated onto matrigel-coated dishes (BD). Once iPSCs reached a confluence of 100%, neural differentiation was initiated by adding knockout serum replacement medium supplemented with the SMAD pathway inhibitors SB431542 (Tocris Bioscience) and LDN-193189 (Stemgent). During the first 20 d, several growth factors and small molecules were added to the cell culture medium at various time points as indicated in the previously published protocol (Kriks et al., 2011) to pattern the neurons into the dopaminergic lineage (floor plate induction). On day 21 of the differentiation, cells were dissociated using accutase and plated at a high density (50-µl drop with 350,000 cells) onto the center of culture dishes, which had been previously coated with poly-D-lysine (Sigma-Aldrich) and laminin (Roche), in medium for terminal differentiation (Kriks et al., 2011). Neurons were aged for ∼50 d.

Feeding experiments

1-d-old adult flies were placed on molasses medium supplemented with 100 µM Cerulenin (Enzo Life Sciences), 3 µM Irgasan (Sigma-Aldrich), or 100 µM Orlistat (Sigma-Aldrich), unless otherwise indicated in Fig. 2 (B, D, and F; 2.5% final ethanol concentration), or flies were supplemented with 2.5% ethanol for control medium. The animals were kept on these media for 72 h and tested for flight or ATP levels. To determine mitochondrial morphology, embryos were placed in molasses medium supplemented with 100 µM Cerulenin (2.5% final ethanol concentration) or with 2.5% ethanol for control medium and grown to the third instar larval stage. These third instar larvae were dissected and used for experiments (see Determination of mitochondrial morphology).

To assess ATP levels in the cells, cells were treated with 10 µM Cerulenin for 24 h (0.1% ethanol) or with control medium supplemented with 0.1% ethanol. For Western blotting analysis, wild-type MEFs were treated with 100 µM H_2O_2 for 30 min.

Flight and survival

The flight assay was conducted on male flies using batches of five flies each. The flies were placed in an empty vial and gently tapped. The flies that were able to fly were given a score of 1, whereas those that did not fly were given a score of 0.

For survival, the latest survival stage of animals is indicated for animals that were reared on grape juice plates with yeast paste in uncrowded conditions.

ATP determination

ATP levels were determined as previously described (Park et al., 2006; Morais et al., 2014) using an ATP determination kit (Invitrogen) according to the supplier's protocol. Luminescence was measured on a luminometer (Bio-Rad Laboratories), and values were normalized to total protein content using the Bradford method.

Mitochondrial isolation and complex I activity measurements

Flies and cells were homogenized in 1-ml chilled mitochondrial isolation medium (Abcam) and then spun twice at 1,000 *g* for 5 min. The supernatant was collected and spun at 13,000 *g* for 5 min followed by a washing step of the pellet containing the mitochondria with 1 ml of mitochondrial isolation medium and was resuspended in 50 µl isolation medium. The samples were kept at 4°C during the entire process (Walker et al., 2006; Frezza et al., 2007). Mitochondrial isolates were sonicated (10 pulses at 20%) and used to measure complex I activity as previously described (Fischer et al., 1986; de Paepe et al., 2006). In brief, to measure NADH:O_2 oxidoreductase activity, mitochondrial isolates were buffered in medium containing phosphate buffer (0.1 M, pH 7.4), BSA (10 mg/ml), NADH (1 mM), and KCN (30 mM). Decylubiquinone, a ubiquinone analogue, was added to accept the electrons from complex I and to activate the reaction. The activity of NADH oxidation was spectrophotometrically followed at 340 nm at 37°C and was corrected for rotenone-insensitive NADH oxidation. Values were normalized to citrate synthase activity.

For phospholipid incubation, isolated mitochondria underwent freeze-thaw steps and sonication and were then incubated for 60 min with various concentrations of the different lipids at 37°C before complex I activity measurements. The phospholipid analysis revealed that the monounsaturated fatty acyl chains are most abundant (except for CL). Therefore, the following phospholipids were used: CL (LM-6003), PC (850457C), PG (840457C), and PE (850757C).

Western blotting

Cells were collected and diluted in Laemmli sample buffer and were boiled for 5 min. 15 µg of proteins were separated on precast 4–12% NuPage Bis-Tris gels (Invitrogen). Blots were probed with the following primary antibodies: 1:1,000 rabbit anti-FASN and 1:1,000 anti–β-actin

Downloaded from on February 15, 2017

Published January 30, 2017

(Abcam). The membranes were developed with Western Lightning ECL (PerkinElmer) and imaged. Quantification was performed using the gel analyzer tool in ImageJ software (National Institutes of Health).

Determination of mitochondrial morphology

Larvae were dissected in HL-3 (Stewart et al., 1994) and larval fillets were fixed in 4% formaldehyde in PBS for 20 min and permeabilized with 0.4% Triton X-100. Primary antibody monoclonal mouse anti-ATP synthase B (1:200; Abcam) was used to visualize mitochondria. We used goat anti-mouse Alexa Fluor 555 (1:1,000) as a secondary antibody. Images were visualized with a confocal microscope (A1R) through a near-infrared Apo 60× 1.0 NA water dipping lens (Nikon) in room temperature. Images were acquired using the NIS-Elements Advanced Research software package (Nikon). Images were quantified using the analyzing particles plugin in ImageJ, with which rounded mitochondria were automatically detected and counted.

Electron microscopy

Electron microscopic analyses of thorax mitochondria were performed as previously described (Esposito et al., 2013). In brief, thoraxes of adult flies were fixed in paraformaldehyde/glutaraldehyde, postfixed in osmium tetroxide, dehydrated, and embedded in epon. 80-nm-thick sections were stained with uranylacetate end lead citrate, sections were imaged using a transmission electron microscope (TEM 1400; JEOL) at room temperature and a bottom-mounted camera (11 MP; Quemesa; Olympus), and iTEM 5.2 software (ResAlta Research Technologies) was used to acquire micrographs. Mitochondrial morphology was analyzed using ImageJ and scored in a blinded fashion as normal mitochondria with organized cristae or as swollen mitochondria devoid of cristae from five flies. For each fly, five sections were analyzed.

Free fatty acid measurement

30 adult flies were homogenized in 5% isopropanol and 5% Triton X-100 and prepared according to the manufacturer's protocol (BioAssay Systems). The amount of free fatty acids was analyzed by measuring optic density at 570 nm on a Multilabel reader (Biotek). Values were normalized to protein content.

Free palmitate measurement

One million cells were plated in 6-well plates and incubated with Cerulenin for 24 h before sample collection. Metabolites for the subsequent mass spectrometry analysis were prepared by quenching the cells in liquid nitrogen followed by a cold two-phase methanol/water/chloroform extraction (Christen et al., 2016). During the extraction, samples were constantly refrigerated in a dry ice/ice mixture. Each sample was scraped in 800 µl of a 3:5 water/methanol solution and collected in a 1.5-ml tube. Norvaline (0.75 µg/sample) and glutarate (0.75 µg/sample) were added as internal standards for polar metabolites. Next, 500 µl chloroform was added to each sample. Heptadecanoate (5 µg/sample) was also added as an internal standard for fatty acids. Samples were vortexed for 10 min at 4°C, and phase separation was then achieved by centrifugation at 4°C at maximum speed for 10 min on a refrigerated bench-top centrifuge. The water/methanol phase containing polar metabolites, the chloroform phase containing fatty acids, and the interphase containing proteins and DNA were separated and dried using a vacuum concentrator. Dried metabolite samples were stored at −80°C until further processing. Fatty acids were esterified with 2% sulfuric acid in methanol, shaken for 15 min at room temperature, and subsequently extracted by addition of 600 µl hexane and 100 µl of saturated NaCl per sample, followed by vortexing for 10 min and centrifugation at 4°C at maximum speed for 5 min on a refrigerated bench-top centrifuge. The hexane (upper) phase was transferred to new 1.5-ml tubes and dried using a vacuum concentrator. Samples were then resuspended in 25–100 µl hexane, vortexed for 10 min, and transferred to glass vials for gas chromatography–mass spectrometry analysis. The method was tested on free fatty acid and triglyceride standards and was verified to specifically esterify free fatty acids. Metabolite levels were measured with a gas chromatography system (7890A) combined with an inert mass spectrometry system (5975C; Agilent Technologies) as described previously (Lorendeau et al., 2016). Specifically, 1 µl of sample was injected into a DB35MS column (Agilent Technologies) in splitless mode using an inlet temperature of 270°C. The carrier gas was helium with a flow rate of 1 ml/min. Upon injection, the gas chromatography oven was held at 80°C for 1 min and then ramped with 5°C/min to 300°C. The mass spectrometry system was operated under electron impact ionization at 70 eV, and a mass range of 100–650 atomic mass units was scanned. The palmitate peak was identified based on a standard curve, and the area under the curve of the palmitate peak was integrated using a MatLab M file, published by Young et al. (2008), which applies consistent integration bounds and baseline correction to each ion. The total ion counts for palmitate of each sample was compared with a blank extraction without cells to correct for the eventual presence of noncellular tracers of palmitate. The data were normalized over total DNA content. For this purpose, total DNA was extracted from the interphase with the DNeasy Blood and Tissue kit (QIAGEN) and quantified with a spectrophotometer (Nanodrop 2000; Thermo Fisher Scientific).

Lipid extraction for mass spectrometry lipidomics

Mass spectrometry–based lipid analysis was performed at Lipotype GmbH as described previously (Sampaio et al., 2011). Lipids were extracted using a two-step chloroform/methanol procedure (Ejsing et al., 2009). Samples were spiked with internal lipid standard mixture containing CL 16:1/15:0/15:0/15:0, ceramide 18:1:2/17:0, diacylglycerol 17:0/17:0, hexosyl ceramide 18:1:2/12:0, lysophosphatidate 17:0, lysophosphatidyl choline 12:0, lysophosphatidyl ethanolamine 17:1, lysophosphatidyl glycerol 17:1, lysophosphatidyl inositol 17:1, lysophosphatidyl serine 17:1, phosphatidate 17:0/17:0, PC 17:0/17:0, PE 17:0/17:0, PG 17:0/17:0, phosphatidyl inositol 16:0/16:0, phosphatidyl serine 17:0/17:0, cholesterol ester 20:0, sphingomyelin 18:1:2/12:0:0, triacylglycerol 17:0/17:0/17:0, and cholesterol D6. After extraction, the organic phase was transferred to an infusion plate and dried in a speed vacuum concentrator. First-step dry extract was resuspended in 7.5 mM ammonium acetate in chloroform/methanol/propanol (1:2:4; V:V:V), and second-step dry extract was resuspended in 33% ethanol solution of methylamine in chloroform/methanol (0.003:5:1; V:V:V). All liquid handling steps were performed using the STARlet robotic platform with the Anti-Droplet Control feature for organic solvents pipetting (Hamilton Robotics).

Mass spectrometry data acquisition

Samples were analyzed by direct infusion on a mass spectrometer (QExactive; Thermo Fisher Scientific) equipped with an ion source (TriVersa NanoMate; Advion Biosciences). Samples were analyzed in both positive and negative ion modes with a resolution of mass/charge ratio = 200 = 280,000 for mass spectrometry and Rm/z = 200 = 17,500 for tandem mass spectrometry experiments in a single acquisition. tandem mass spectrometry was triggered by an inclusion list encompassing corresponding mass spectrometry mass ranges scanned in 1-D increments (Surma et al., 2015). Both mass spectrometry and tandem mass spectrometry data were combined to monitor CE, diacylglycerol, and triacylglycerol ions as ammonium adducts; PC and PC O^- as acetate adducts; and CL, phosphatidate, PE, PE O^-, PG, phosphatidyl inositol, and phosphatidyl serine as deprotonated anions. Mass

Downloaded from on February 15, 2017

Published January 30, 2017

spectrometry only was used to monitor lysophosphatidate, lysophosphatidyl ethanolamine, lysophosphatidyl ethanolamine O^-, lysophosphatidyl inositol, and lysophosphatidyl serine as deprotonated anions; ceramide, hexosyl ceramide, sphingomyelin, lysophosphatidyl choline, and lysophosphatidyl choline O^- as acetate adduct; and cholesterol as an ammonium adduct of an acetylated derivative (Liebisch et al., 2006).

Data analysis and postprocessing

Data were analyzed with in-house developed lipid identification software based on LipidXplorer (Herzog et al., 2011, 2012). Data postprocessing and normalization were performed using an in-house developed data management system. Only lipid identifications with a signal-to-noise ratio of >5 and a signal intensity fivefold higher than in corresponding blank samples were considered for further data analysis.

Statistics

Statistical analyses was performed using Prism software (GraphPad), and to assess whether the observed data points were significantly different, we used a two-tailed Student's *t* test when comparing two conditions or one-way analysis of variance with Bonferroni's post-hoc test when comparing more than two conditions. P-values were considered significant when they were <0.05.

Online supplemental material

Fig. S1 shows the identification of the suppressive alleles in *pink1*^{B9} mutant flies. Fig. S2 shows that inhibition of FASN results in the suppression of *pink1*^{B9} mutant flies, but not in the suppression of Parkin mutant flies. Fig. S3 shows the levels of various phospholipids in *Pink1*$^{-/-}$ MEFs upon inhibition of FASN. Fig. S4 shows the complex I activity of *pink1* mutant flies that were pretreated with stearic acid.

Acknowledgments

We thank G. Marschner, F. Rudolph, R. Goodchild, H. Bellen, J. Park, J. Chung, and the Bloomington Drosophila Stock Center.

Support was provided by a Fonds Wetenschappelijk Onderzoek and European Molecular Biology Organization stipend to M. Vos (ALTF 851-2014), a European Research Council Starting and Consolidator grant to P. Verstreken (ERC-2014-CoG–646671), Fonds Wetenschappelijk Onderzoek grants (G0D3417N, G0D3317N, G088515N, and G094915N), an Interuniversitaire Attractie Pool by Federaal Wetenschapsbeleid (P7/16), the Research Fund Katholieke Universiteit Leuven, a Methusalem grant from the Flemish government, the Hercules Foundation, Opening the Future, Deutsche Forschungsgemeinschaft (KL1134/11-1), and the Vlaams Instituut voor Biotechnologie. B. De Strooper is a paid consultant for and P. Verstreken receives research funding from Janssen Pharmaceuticals. C. Klein is the recipient of a career development award from the Hermann and Lilly Schilling Foundation.

The authors declare no further competing financial interests.

Author contributions: Conceptualization, methodology, and writing: M. Vos and P. Verstreken; investigation: M. Vos, A. Geens, C. Böhm, L. Deaulmerie, J. Swerts, M. Rossi, K. Craessaerts, E.P. Leites, P. Seibler, A. Rakovic, T. Lohnau, and V.A. Morais; supervision, review, and editing: M. Vos, B. De Strooper, S.-M. Fendt, V.A. Morais, C. Klein, and P. Verstreken.

Submitted: 11 November 2015
Revised: 25 November 2016
Accepted: 5 January 2017

References

Acehan, D., A. Malhotra, Y. Xu, M. Ren, D.L. Stokes, and M. Schlame. 2011. Cardiolipin affects the supramolecular organization of ATP synthase in mitochondria. *Biophys. J.* 100:2184–2192. http://dx.doi.org/10.1016/j.bpj.2011.03.031

Aoun, M., and V. Tiranti. 2015. Mitochondria: a crossroads for lipid metabolism defect in neurodegeneration with brain iron accumulation diseases. *Int. J. Biochem. Cell Biol.* 63:25–31. http://dx.doi.org/10.1016/j.biocel.2015.01.018

Ashburner, M., P. Thompson, J. Roote, P.F. Lasko, Y. Grau, M. el Messal, S. Roth, and P. Simpson. 1990. The genetics of a small autosomal region of Drosophila melanogaster containing the structural gene for alcohol dehydrogenase. VII. Characterization of the region around the snail and cactus loci. *Genetics.* 126:679–694.

Bier, E., H. Vaessin, S. Shepherd, K. Lee, K. McCall, S. Barbel, L. Ackerman, R. Carretto, T. Uemura, E. Grell, et al. 1989. Searching for pattern and mutation in the Drosophila genome with a P-lacZ vector. *Genes Dev.* 3:1273–1287. http://dx.doi.org/10.1101/gad.3.9.1273

Bobyleva, V., M. Bellei, T.L. Pazienza, and U. Muscatello. 1997. Effect of cardiolipin on functional properties of isolated rat liver mitochondria. *Biochem. Mol. Biol. Int.* 41:469–480.

Buratta, M., E. Castigli, M. Sciaccaluga, R.M. Pellegrino, F. Spinozzi, R. Roberti, and L. Corazzi. 2008. Loss of cardiolipin in palmitate-treated GL15 glioblastoma cells favors cytochrome *c* release from mitochondria leading to apoptosis. *J. Neurochem.* 105:1019–1031. http://dx.doi.org/10.1111/j.1471-4159.2007.05209.x

Cha, G.-H., S. Kim, J. Park, E. Lee, M. Kim, S.B. Lee, J.M. Kim, J. Chung, and K.S. Cho. 2005. Parkin negatively regulates JNK pathway in the dopaminergic neurons of *Drosophila*. *Proc. Natl. Acad. Sci. USA.* 102:10345–10350. http://dx.doi.org/10.1073/pnas.0500346102

Chirala, S.S., and S.J. Wakil. 2004. Structure and function of animal fatty acid synthase. *Lipids.* 39:1045–1053. http://dx.doi.org/10.1007/s11745-004-1329-9

Christen, S., D. Lorendeau, R. Schmieder, D. Broekaert, K. Metzger, K. Veys, I. Elia, J.M. Buescher, M.F. Orth, S.M. Davidson, et al. 2016. Breast cancer-derived lung metastases show increased pyruvate carboxylase-dependent anaplerosis. *Cell Reports.* 17:837–848. http://dx.doi.org/10.1016/j.celrep.2016.09.042

Chu, C.T., J. Ji, R.K. Dagda, J.F. Jiang, Y.Y. Tyurina, A.A. Kapralov, V.A. Tyurin, N. Yanamala, I.H. Shrivastava, D. Mohammadyani, et al. 2013. Cardiolipin externalization to the outer mitochondrial membrane acts as an elimination signal for mitophagy in neuronal cells. *Nat. Cell Biol.* 15:1197–1205. http://dx.doi.org/10.1038/ncb2837

Clark, I.E., M.W. Dodson, C. Jiang, J.H. Cao, J.R. Huh, J.H. Seol, S.J. Yoo, B.A. Hay, and M. Guo. 2006. *Drosophila pink1* is required for mitochondrial function and interacts genetically with *parkin*. *Nature.* 441:1162–1166. http://dx.doi.org/10.1038/nature04779

de Paepe, B., J. Smet, J.G. Leroy, S. Seneca, E. George, D. Matthys, L. van Maldergem, E. Scalais, W. Lissens, L. de Meirleir, et al. 2006. Diagnostic value of immunostaining in cultured skin fibroblasts from patients with oxidative phosphorylation defects. *Pediatr. Res.* 59:2–6. http://dx.doi.org/10.1203/01.pdr.0000191294.34122.ab

Ejsing, C.S., J.L. Sampaio, V. Surendranath, E. Duchoslav, K. Ekroos, R.W. Klemm, K. Simons, and A. Shevchenko. 2009. Global analysis of the yeast lipidome by quantitative shotgun mass spectrometry. *Proc. Natl. Acad. Sci. USA.* 106:2136–2141. http://dx.doi.org/10.1073/pnas.0811700106

Ellis, C.E., E.J. Murphy, D.C. Mitchell, M.Y. Golovko, F. Scaglia, G.C. Barceló-Coblijn, and R.L. Nussbaum. 2005. Mitochondrial lipid abnormality and electron transport chain impairment in mice lacking α-synuclein. *Mol. Cell. Biol.* 25:10190–10201. http://dx.doi.org/10.1128/MCB.25.22.10190-10201.2005

Esposito, G., M. Vos, S. Vilain, J. Swerts, J. De Sousa Valadas, S. Van Meensel, O. Schaap, and P. Verstreken. 2013. Aconitase causes iron toxicity in *Drosophila pink1* mutants. *PLoS Genet.* 9. http://dx.doi.org/10.1371/journal.pgen.1003478

Filippov, V., M.A. Song, K. Zhang, H.V. Vinters, S. Tung, W.M. Kirsch, J. Yang, and P.J. Duerksen-Hughes. 2012. Increased ceramide in brains with Alzheimer's and other neurodegenerative diseases. *J. Alzheimers Dis.* 29:537–547.

Fischer, J.C., W. Ruitenbeek, F.J. Gabreëls, A.J.M. Janssen, W.O. Renier, R.C.A. Sengers, A.M. Stadhouders, H.J. ter Laak, J.M.F. Trijbels, and J.H. Veerkamp. 1986. A mitochondrial encephalomyopathy: the first case with an established defect at the level of coenzyme Q. *Eur. J. Pediatr.* 144:441–444. http://dx.doi.org/10.1007/BF00441735

Frezza, C., S. Cipolat, and L. Scorrano. 2007. Organelle isolation: functional mitochondria from mouse liver, muscle and cultured fibroblasts. *Nat. Protoc.* 2:287–295. http://dx.doi.org/10.1038/nprot.2006.478

Downloaded from on February 15, 2017

Published January 30, 2017

Friedman, J.R., A. Mourier, J. Yamada, J.M. McCaffery, and J. Nunnari. 2015. MICOS coordinates with respiratory complexes and lipids to establish mitochondrial inner membrane architecture. *eLife.* 4. http://dx.doi.org/10.7554/eLife.07739

Garcia Fernandez, M., L. Troiano, L. Moretti, M. Nasi, M. Pinti, S. Salvioli, J. Dobrucki, and A. Cossarizza. 2002. Early changes in intramitochondrial cardiolipin distribution during apoptosis. *Cell Growth Differ.* 13:449–455.

Garrido, D., T. Rubin, M. Poidevin, B. Maroni, A. Le Rouzic, J.-P. Parvy, and J. Montagne. 2015. Fatty acid synthase cooperates with glyoxalase 1 to protect against sugar toxicity. *PLoS Genet.* 11. http://dx.doi.org/10.1371/journal.pgen.1004995

Gautier, C.A., T. Kitada, and J. Shen. 2008. Loss of PINK1 causes mitochondrial functional defects and increased sensitivity to oxidative stress. *Proc. Natl. Acad. Sci. USA.* 105:11364–11369. http://dx.doi.org/10.1073/pnas.0802076105

Grünewald, A., M.E. Gegg, J.W. Taanman, R.H. King, N. Kock, C. Klein, and A.H.V. Schapira. 2009. Differential effects of PINK1 nonsense and missense mutations on mitochondrial function and morphology. *Exp. Neurol.* 219:266–273. http://dx.doi.org/10.1016/j.expneurol.2009.05.027

Haddad, D.M., S. Vilain, M. Vos, G. Esposito, S. Matta, V.M. Kalscheuer, K. Craessaerts, M. Leyssen, R.M. Nascimento, A.M. Vianna-Morgante, et al. 2013. Mutations in the intellectual disability gene *Ube2a* cause neuronal dysfunction and impair parkin-dependent mitophagy. *Mol. Cell.* 50:831–843. http://dx.doi.org/10.1016/j.molcel.2013.04.012

He, Y., K.W. Leung, Y.-H. Zhang, S. Duan, X.-F. Zhong, R.-Z. Jiang, Z. Peng, J. Tombran-Tink, and J. Ge. 2008. Mitochondrial complex I defect induces ROS release and degeneration in trabecular meshwork cells of POAG patients: protection by antioxidants. *Invest. Ophthalmol. Vis. Sci.* 49:1447–1458. http://dx.doi.org/10.1167/iovs.07-1361

Herzog, R., D. Schwudke, K. Schuhmann, J.L. Sampaio, S.R. Bornstein, M. Schroeder, and A. Shevchenko. 2011. A novel informatics concept for high-throughput shotgun lipidomics based on the molecular fragmentation query language. *Genome Biol.* 12. http://dx.doi.org/10.1186/gb-2011-12-1-r8

Herzog, R., K. Schuhmann, D. Schwudke, J.L. Sampaio, S.R. Bornstein, M. Schroeder, and A. Shevchenko. 2012. LipidXplorer: a software for consensual cross-platform lipidomics. *PLoS One.* 7. http://dx.doi.org/10.1371/journal.pone.0029851

Hoch, F.L. 1992. Cardiolipins and biomembrane function. *Biochim. Biophys. Acta.* 1113:71–133. http://dx.doi.org/http://dx,10.1016/0304-4157(92)90035-9

Jazvinšćak Jembrek, M., P.R. Hof, and G. Šimić. 2015. Ceramides in Alzheimer's disease: key mediators of neuronal apoptosis induced by oxidative stress and Aβ accumulation. *Oxid. Med. Cell. Longev.* 2015. http://dx.doi.org/10.1155/2015/346783

Kapoor, M., C.C. Reddy, M.V. Krishnasastry, N. Surolia, and A. Surolia. 2004. Slow-tight-binding inhibition of enoyl-acyl carrier protein reductase from *Plasmodium falciparum* by triclosan. *Biochem. J.* 381:719–724. http://dx.doi.org/10.1042/BJ20031821

Kriks, S., J.-W. Shim, J. Piao, Y.M. Ganat, D.R. Wakeman, Z. Xie, L. Carrillo-Reid, G. Auyeung, C. Antonacci, A. Buch, et al. 2011. Dopamine neurons derived from human ES cells efficiently engraft in animal models of Parkinson's disease. *Nature.* 480:547–551.

Liebisch, G., M. Binder, R. Schifferer, T. Langmann, B. Schulz, and G. Schmitz. 2006. High throughput quantification of cholesterol and cholesteryl ester by electrospray ionization tandem mass spectrometry (ESI-MS/MS). *Biochim. Biophys. Acta.* 1761:121–128. http://dx.doi.org/10.1016/j.bbalip.2005.12.007

Lim, L., V. Jackson-Lewis, L.C. Wong, G.H. Shui, A.X.H. Goh, S. Kesavapany, A.M. Jenner, M. Fivaz, S. Przedborski, and M.R. Wenk. 2012. Lanosterol induces mitochondrial uncoupling and protects dopaminergic neurons from cell death in a model for Parkinson's disease. *Cell Death Differ.* 19:416–427. http://dx.doi.org/10.1038/cdd.2011.105

Lorendeau, D., G. Rinaldi, R. Boon, P. Spincemaille, K. Metzger, C. Jäger, S. Christen, X. Dong, S. Kuenen, K. Voordeckers, et al. 2016. Dual loss of succinate dehydrogenase (SDH) and complex I activity is necessary to recapitulate the metabolic phenotype of SDH mutant tumors. *Metab. Eng.* In press. http://dx.doi.org/10.1016/j.ymben.2016.11.005

Mason, J.M., J. Ransom, and A.Y. Konev. 2004. A deficiency screen for dominant suppressors of telomeric silencing in Drosophila. *Genetics.* 168:1353–1370. http://dx.doi.org/10.1534/genetics.104.030676

Menendez, J.A., and R. Lupu. 2007. Fatty acid synthase and the lipogenic phenotype in cancer pathogenesis. *Nat. Rev. Cancer.* 7:763–777. http://dx.doi.org/10.1038/nrc2222

Morais, V.A., P. Verstreken, A. Roethig, J. Smet, A. Snellinx, M. Vanbrabant, D. Haddad, C. Frezza, W. Mandemakers, D. Vogt-Weisenhorn, et al. 2009. Parkinson's disease mutations in PINK1 result in decreased Complex I activity and deficient synaptic function. *EMBO Mol. Med.* 1:99–111. http://dx.doi.org/10.1002/emmm.200900006

Morais, V.A., D. Haddad, K. Craessaerts, P.-J. De Bock, J. Swerts, S. Vilain, L. Aerts, L. Overbergh, A. Grünewald, P. Seibler, et al. 2014. PINK1 loss-of-function mutations affect mitochondrial complex I activity via NdufA10 ubiquinone uncoupling. *Science.* 344:203–207. http://dx.doi.org/10.1126/science.1249161

Munsie, L.N., A.J. Milnerwood, P. Seibler, D.A. Beccano-Kelly, I. Tatarnikov, J. Khinda, M. Volta, C. Kadgien, L.P. Cao, L. Tapia, et al. 2015. Retromer-dependent neurotransmitter receptor trafficking to synapses is altered by the Parkinson's disease VPS35 mutation p.D620N. *Hum. Mol. Genet.* 24:1691–1703. http://dx.doi.org/10.1093/hmg/ddu582

Narendra, D., A. Tanaka, D.F. Suen, and R.J. Youle. 2009. Parkin-induced mitophagy in the pathogenesis of Parkinson disease. *Autophagy.* 5:706–708. http://dx.doi.org/10.4161/auto.5.5.8505

Narendra, D.P., S.M. Jin, A. Tanaka, D.F. Suen, C.A. Gautier, J. Shen, M.R. Cookson, and R.J. Youle. 2010. PINK1 is selectively stabilized on impaired mitochondria to activate Parkin. *PLoS Biol.* 8. http://dx.doi.org/10.1371/journal.pbio.1000298

Nguyen, P.L., J. Ma, J.E. Chavarro, M.L. Freedman, R. Lis, G. Fedele, C. Fiore, W. Qiu, M. Fiorentino, S. Finn, et al. 2010. Fatty acid synthase polymorphisms, tumor expression, body mass index, prostate cancer risk, and survival. *J. Clin. Oncol.* 28:3958–3964. http://dx.doi.org/10.1200/JCO.2009.27.0793

Nowicki, M., F. Müller, and M. Frentzen. 2005. Cardiolipin synthase of *Arabidopsis thaliana*. *FEBS Lett.* 579:2161–2165. http://dx.doi.org/10.1016/j.febslet.2005.03.007

Ogino, S., K. Nosho, J.A. Meyerhardt, G.J. Kirkner, A.T. Chan, T. Kawasaki, E.L. Giovannucci, M. Loda, and C.S. Fuchs. 2008. Cohort study of fatty acid synthase expression and patient survival in colon cancer. *J. Clin. Oncol.* 26:5713–5720. http://dx.doi.org/10.1200/JCO.2008.18.2675

Omura, S. 1976. The antibiotic cerulenin, a novel tool for biochemistry as an inhibitor of fatty acid synthesis. *Bacteriol. Rev.* 40:681–697.

Ostrander, D.B., G.C. Sparagna, A.A. Amoscato, J.B. McMillin, and W. Dowhan. 2001. Decreased cardiolipin synthesis corresponds with cytochrome *c* release in palmitate-induced cardiomyocyte apoptosis. *J. Biol. Chem.* 276:38061–38067.

Park, J., S.B. Lee, S. Lee, Y. Kim, S. Song, S. Kim, E. Bae, J. Kim, M. Shong, J.-M. Kim, and J. Chung. 2006. Mitochondrial dysfunction in *Drosophila PINK1* mutants is complemented by *parkin*. *Nature.* 441:1157–1161. http://dx.doi.org/10.1038/nature04788

Park, J., S.E. Lee, J. Hur, E.B. Hong, J.-I. Choi, J.-M. Yang, J.-Y. Kim, Y.-C. Kim, H.-J. Cho, J.M. Peters, et al. 2015. M-CSF from cancer cells induces fatty acid synthase and PPARβ/δ activation in tumor myeloid cells, leading to tumor progression. *Cell Reports.* 10:1614–1625. http://dx.doi.org/10.1016/j.celrep.2015.02.024

Parks, A.L., K.R. Cook, M. Belvin, N.A. Dompe, R. Fawcett, K. Huppert, L.R. Tan, C.G. Winter, K.P. Bogart, J.E. Deal, et al. 2004. Systematic generation of high-resolution deletion coverage of the *Drosophila melanogaster* genome. *Nat. Genet.* 36:288–292. http://dx.doi.org/10.1038/ng1312

Pesah, Y., T. Pham, H. Burgess, B. Middlebrooks, P. Verstreken, Y. Zhou, M. Harding, H. Bellen, and G. Mardon. 2004. *Drosophila parkin* mutants have decreased mass and cell size and increased sensitivity to oxygen radical stress. *Development.* 131:2183–2194. http://dx.doi.org/10.1242/dev.01095

Pfeiffer, K., V. Gohil, R.A. Stuart, C. Hunte, U. Brandt, M.L. Greenberg, and H. Schägger. 2003. Cardiolipin stabilizes respiratory chain supercomplexes. *J. Biol. Chem.* 278:52873–52880. http://dx.doi.org/10.1074/jbc.M308366200

Pogson, J.H., R.M. Ivatt, A. Sanchez-Martinez, R. Tufi, E. Wilson, H. Mortiboys, and A.J. Whitworth. 2014. The complex I subunit *NDUFA10* selectively rescues *Drosophila pink1* mutants through a mechanism independent of mitophagy. *PLoS Genet.* 10. http://dx.doi.org/10.1371/journal.pgen.1004815

Poole, A.C., R.E. Thomas, L.A. Andrews, H.M. McBride, A.J. Whitworth, and L.J. Pallanck. 2008. The PINK1/Parkin pathway regulates mitochondrial morphology. *Proc. Natl. Acad. Sci. USA.* 105:1638–1643. http://dx.doi.org/10.1073/pnas.0709336105

Rakovic, A., K. Shurkewitsch, P. Seibler, A. Grünewald, A. Zanon, J. Hagenah, D. Krainc, and C. Klein. 2013. Phosphatase and tensin homolog (PTEN)-induced putative kinase 1 (PINK1)-dependent ubiquitination of endogenous Parkin attenuates mitophagy: study in human primary fibroblasts and induced pluripotent stem cell-derived neurons. *J. Biol. Chem.* 288:2223–2237. http://dx.doi.org/10.1074/jbc.M112.391680

Ruggiero, F.M., F. Cafagna, V. Petruzzella, M.N. Gadaleta, and E. Quagliariello. 1992. Lipid composition in synaptic and nonsynaptic mitochondria from rat brains and effect of aging. *J. Neurochem.* 59:487–491. http://dx.doi.org/10.1111/j.1471-4159.1992.tb09396.x

Downloaded from on February 15, 2017

Published January 30, 2017

Ryder, E., M. Ashburner, R. Bautista-Llacer, J. Drummond, J. Webster, G. Johnson, T. Morley, Y.S. Chan, F. Blows, D. Coulson, et al. 2007. The DrosDel deletion collection: a Drosophila genomewide chromosomal deficiency resource. *Genetics.* 177:615–629. http://dx.doi.org/10.1534/genetics.107.076216

Rytömaa, M., and P.K. Kinnunen. 1994. Evidence for two distinct acidic phospholipid-binding sites in cytochrome *c*. *J. Biol. Chem.* 269:1770–1774.

Sampaio, J.L., M.J. Gerl, C. Klose, C.S. Ejsing, H. Beug, K. Simons, and A. Shevchenko. 2011. Membrane lipidome of an epithelial cell line. *Proc. Natl. Acad. Sci. USA.* 108:1903–1907. http://dx.doi.org/10.1073/pnas.1019267108

Senyilmaz, D., S. Virtue, X. Xu, C.Y. Tan, J.L. Griffin, A.K. Miller, A. Vidal-Puig, and A.A. Teleman. 2015. Regulation of mitochondrial morphology and function by stearoylation of TFR1. *Nature.* 525:124–128. http://dx.doi.org/10.1038/nature14601

Spradling, A.C., D. Stern, A. Beaton, E.J. Rhem, T. Laverty, N. Mozden, S. Misra, and G.M. Rubin. 1999. The Berkeley Drosophila Genome Project gene disruption project: Single *P*-element insertions mutating 25% of vital Drosophila genes. *Genetics.* 153:135–177.

Stewart, B.A., H.L. Atwood, J.J. Renger, J. Wang, and C.F. Wu. 1994. Improved stability of *Drosophila* larval neuromuscular preparations in haemolymph-like physiological solutions. *J. Comp. Physiol. A Neuroethol. Sens. Neural Behav. Physiol.* 175:179–191. http://dx.doi.org/10.1007/BF00215114

Surma, M.A., R. Herzog, A. Vasilj, C. Klose, N. Christinat, D. Morin-Rivron, K. Simons, M. Masoodi, and J.L. Sampaio. 2015. An automated shotgun lipidomics platform for high throughput, comprehensive, and quantitative analysis of blood plasma intact lipids. *Eur. J. Lipid Sci. Technol.* 117:1540–1549. http://dx.doi.org/10.1002/ejlt.201500145

Tyurina, Y.Y., A.M. Polimova, E. Maciel, V.A. Tyurin, V.I. Kapralova, D.E. Winnica, A.S. Vikulina, M.R.M. Domingues, J. McCoy, L.H. Sanders, et al. 2015. LC/MS analysis of cardiolipins in substantia nigra and plasma of rotenone-treated rats: implication for mitochondrial dysfunction in Parkinson's disease. *Free Radic. Res.* 49:681–691. http://dx.doi.org/10.3109/10715762.2015.1005085

Valente, E.M., P.M. Abou-Sleiman, V. Caputo, M.M.K. Muqit, K. Harvey, S. Gispert, Z. Ali, D. Del Turco, A.R. Bentivoglio, D.G. Healy, et al. 2004. Hereditary early-onset Parkinson's disease caused by mutations in *PINK1*. *Science.* 304:1158–1160. http://dx.doi.org/10.1126/science.1096284

Verstreken, P., C.V. Ly, K.J.T. Venken, T.-W. Koh, Y. Zhou, and H.J. Bellen. 2005. Synaptic mitochondria are critical for mobilization of reserve pool vesicles at *Drosophila* neuromuscular junctions. *Neuron.* 47:365–378. http://dx.doi.org/10.1016/j.neuron.2005.06.018

Vilain, S., G. Esposito, D. Haddad, O. Schaap, M.P. Dobreva, M. Vos, S. Van Meensel, V.A. Morais, B. De Strooper, and P. Verstreken. 2012. The yeast complex I equivalent NADH dehydrogenase rescues *pink1* mutants. *PLoS Genet.* 8. http://dx.doi.org/10.1371/journal.pgen.1002456

Vos, M., G. Esposito, J.N. Edirisinghe, S. Vilain, D.M. Haddad, J.R. Slabbaert, S. Van Meensel, O. Schaap, B. De Strooper, R. Meganathan, et al. 2012. Vitamin K_2 is a mitochondrial electron carrier that rescues pink1 deficiency. *Science.* 336:1306–1310. http://dx.doi.org/10.1126/science.1218632

Vos, M., B. Lovisa, A. Geens, V.A. Morais, G. Wagnières, H. van den Bergh, A. Ginggen, B. De Strooper, Y. Tardy, and P. Verstreken. 2013. Near-infrared 808 nm light boosts complex IV-dependent respiration and rescues a Parkinson-related *pink1* model. *PLoS One.* 8. http://dx.doi.org/10.1371/journal.pone.0078562

Wakil, S.J., J.K. Stoops, and V.C. Joshi. 1983. Fatty acid synthesis and its regulation. *Annu. Rev. Biochem.* 52:537–579. http://dx.doi.org/10.1146/annurev.bi.52.070183.002541

Walker, D.W., P. Hájek, J. Muffat, D. Knoepfle, S. Cornelison, G. Attardi, and S. Benzer. 2006. Hypersensitivity to oxygen and shortened lifespan in a *Drosophila* mitochondrial complex II mutant. *Proc. Natl. Acad. Sci. USA.* 103:16382–16387. http://dx.doi.org/10.1073/pnas.0607918103

Yang, Y., S. Gehrke, Y. Imai, Z. Huang, Y. Ouyang, J.W. Wang, L. Yang, M.F. Beal, H. Vogel, and B. Lu. 2006. Mitochondrial pathology and muscle and dopaminergic neuron degeneration caused by inactivation of *Drosophila* Pink1 is rescued by Parkin. *Proc. Natl. Acad. Sci. USA.* 103:10793–10798. http://dx.doi.org/10.1073/pnas.0602493103

Young, J.D., K.L. Henne, J.A. Morgan, A.E. Konopka, and D. Ramkrishna. 2008. Integrating cybernetic modeling with pathway analysis provides a dynamic, systems-level description of metabolic control. *Biotechnol. Bioeng.* 100:542–559. http://dx.doi.org/10.1002/bit.21780

Downloaded from on February 15, 2017